Exciton confinement in InAs/InP quantum wires and quantum wells in the presence of a magnetic field

Y. Sidor,[1] B. Partoens,[1] F. M. Peeters,[1] J. Maes,[2] M. Hayne,[3] D. Fuster,[4] Y. González,[4] L. González,[4] and V. V. Moshchalkov[2]

[1]*Departement Fysica, Universiteit Antwerpen (CGB), Groenenborgerlaan 171, B-2020 Antwerpen, Belgium*
[2]*INPAC-Institute for Nanoscale Physics and Chemistry, Pulsed Field Group,*
K.U. Leuven, Celestijnenlaan 200D, B-3001 Leuven, Belgium
[3]*Department of Physics, Lancaster University, Lancaster LAI 4YB, United Kingdom*
[4]*Instituto de Microelectrónica de Madrid (CNM-CSIC), Isaac Newton 8, Tres Cantos, Madrid 28760, Spain*

The charge confinement in InAs/InP based quantum wells and self-assembled quantum wires is investigated theoretically and experimentally through the study of the exciton diamagnetic shift. The numerical calculations are performed within the single-band effective mass approximation, including band nonparabolicity and strain effects. The exciton diamagnetic shift is obtained for quantum wires and quantum wells incorporating local width fluctuations, as well as the electron-hole Coulomb interaction energy. Both electrons and holes (but to a lesser extent) show a substantial penetration into the InP barrier. A detailed comparison is made between the theoretical and experimental data on the magnetic field dependence of the exciton diamagnetic shift. Our theoretical analysis shows that excitons in the InAs/InP quantum well are trapped by local well width fluctuations.

I. INTRODUCTION

The optical properties of quantum nanostructures have been intensively studied to achieve device applications and because they provide the confinement for electrons and holes in such systems. The confinement of the electron and the hole is responsible for the properties of an exciton in such systems. Confinement of the particles depends on the size and shape of the semiconductor nanostructure. It can also be controlled through a selection of structure and barrier materials to obtain various band offsets. Moreover, the application of an external magnetic field can give important information about the carrier confinement.

The magnetoexcitons in a quantum wire (QWR) have been theoretically investigated by a number of authors,[1–3] as was discussed in Ref. 4. An exciton in a quantum well (QW) in the presence of an external magnetic field has been intensively studied over the past decades. For the QW exciton in the presence of an in-plane magnetic field, only a small number of studies have been published[5,6] due to the increased complexity as a consequence of the breaking of the conservation of the total pseudomomentum.[7] Most of the investigations on magnetoexcitons were restricted to the case when the magnetic field is applied along the growth direction (see, for example, Refs. [8–10]). However, all the mentioned studies of the exciton in a perpendicular magnetic field did not include local QW width fluctuations, where excitons (as well as trions and biexcitons) can be trapped.[11–14] Such fluctuations can induce an additional weak lateral confinement, which leads to a confinement of the particles in all three dimensions; i.e., a shallow quantum structure is formed.

One of the promising fabrication methods made it possible to create self-organized nanostructures, formed during the initial stage of heteroepitaxial growth in lattice-mismatched systems. Deposition of InAs on InP by molecular beam epitaxy can lead to a QW or self-assembled quantum wires and dots, depending on the growth conditions. Self-assembled InAs/InP quantum wires and dots are promising candidates for optical applications at telecommunication wavelengths of 1.3 and 1.55 μm,[15–18] among other things because of the enhanced charge confinement as compared to QW. In this paper, we theoretically and experimentally investigate the charge confinement in InAs/InP QW and self-assembled InAs/InP QWRs. Both are designed to emit photoluminescence (PL) around 1.3 μm at room temperature. We report temperature, laser power, and pulsed magnetic field dependence of the PL spectrum. We perform the calculations within the single-band effective mass approximation, but including strain effects and conduction band nonparabolicity. We study the exciton energy shift of QWR and QW with a local thickness fluctuation in magnetic fields up to 50 T and compare theoretical and experimental data.

II. THEORETICAL MODEL

In our calculations, we model the quantum wire as a two-dimensional (2D) quantum box with height h and width w, as shown in Fig. 1(a), and we follow our earlier theoretical approach of Ref. 4. We identify the crystallographic axes [110], [001], and [1$\bar{1}$0] of the InAs/InP self-assembled QWR[4,15,16] with the x, y, and z axes of the wire, and the z axis of the QW with the growth direction of the well (see Fig. 1). For the narrow quantum well of width h, we include a local circular well width fluctuation of 1 ML (monolayer) with radius R, as illustrated in Fig. 1(b).

The single-band effective mass theory is used to calculate the exciton states in both QW and QWR. In our previous work on InAs/InP self-assembled QWR,[4] we presented the basic equations of the QWR in the presence of parallel and perpendicular magnetic fields. In the present work, we ex-
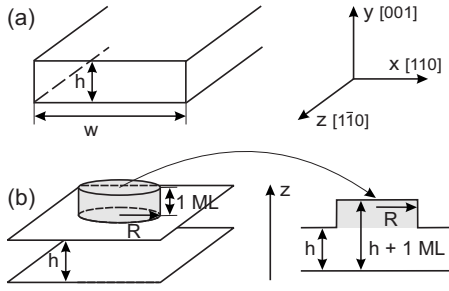
FIG. 1. Schematic drawing of (a) our model of rectangular self-assembled InAs/InP quantum wire with height h and width w, and (b) our model of two-dimensional InAs/InP quantum well with width h. The quantum well width fluctuation of 1 ML and radius R is modeled by the gray area.

tend that work to QW in the presence of parallel and perpendicular magnetic fields and when a local well width fluctuation is present. The components of magnetic field **B** are perpendicular and parallel to the plane motion: $\mathbf{B}=\mathbf{B}_\perp+\mathbf{B}_\parallel$, where $\mathbf{B}_\perp\|\hat{z}$ and $\mathbf{B}_\parallel\perp\hat{z}$. Without going into a detailed description of the basic equations for the QW in the presence of perpendicular and parallel magnetic fields, three points have to be stressed.

(1) The effect of strain on the electron and the hole confinement potentials was included[19,20] by calculating the hydrostatic strain in the conduction and valence bands of the QW, and the shear separation potential in the valence band of the QW. The heavy hole is found to be the ground state in the InAs/InP QW due to the shear separation potential. We include the effect of band nonparabolicity[21] in our calculations by using an energy dependent electron mass

$$m_{nonp.e} = m_e(1 + \alpha E), \tag{1}$$

where m_e and $m_{nonp.e}$ is the bulk and nonparabolic electron mass, respectively, α is the nonparabolicity parameter, which we assume to be[22,23] $\alpha=1.4$ eV^{-1}, and E is the energy of the electron obtained by solving the single-particle Schrödinger equation using the electron bulk mass.

(2) In a parallel magnetic field ($\mathbf{B}_\parallel\perp\hat{z}$), we introduce the center of mass (c.m.) $\mathbf{R}=(m_e\mathbf{r}_e+m_h\mathbf{r}_h)/M$ and relative motion coordinates $\mathbf{r}=\mathbf{r}_e-\mathbf{r}_h$ to describe the exciton state in the QW, where m_e (m_h) denotes the electron (hole) mass, $\mathbf{r}_e$ ($\mathbf{r}_h$) is the electron (hole) coordinates in the xy plane, and $M=m_e+m_h$ is the total mass of the exciton. In the case of a parallel magnetic field, we compare the numerical results for different well widths, but we do not include the local QW width fluctuation [see the dark region in Fig. 1(b)]. This is motivated by the fact that the magnetic field mainly influences the extent of the exciton wave function in the z direction, while a local well width fluctuation will trap the exciton and shift its energy slightly, which will have a very weak magnetic field dependence. This leads to the following Hamiltonian for the exciton:

$$H = -\frac{\hbar^2}{2\mu}\nabla_r^2 - \frac{\hbar^2}{2M}\nabla_R^2 + \frac{i\hbar eB_\parallel}{c}\left(\frac{z_e}{m_e} + \frac{z_h}{m_h}\right)\nabla_{r_y} + \frac{i\hbar eB_\parallel}{Mc}$$

$$\times (z_e - z_h)\nabla_{R_y} + \frac{e^2B_\parallel^2}{2c^2}\left(\frac{z_e^2}{m_e} + \frac{z_h^2}{m_h}\right) - \nabla_{ze}\frac{\hbar^2}{2m_e(z_e)}\nabla_{ze}$$

$$- \nabla_{zh}\frac{\hbar^2}{2m_h(z_h)}\nabla_{zh} + V_e(z_e) + V_h(z_h) - \frac{e^2}{\varepsilon\sqrt{r^2 + (z_e - z_h)^2}}, \tag{2}$$

where $\mu=m_em_h/M$ denotes the exciton reduced mass in the xy plane, $\mathbf{p}=-i\hbar\nabla_r$ is the relative mass momentum in the xy plane, $\mathbf{P}=-i\hbar\nabla_R$ is the exciton c.m. momentum in the xy plane, $V_e(z_e)$ [$V_h(z_h)$] the confinement potential of the electron (hole) along the growth direction of the QW, e is the free-electron charge, and ε is the dielectric constant. Further, the total in-plane pseudomomentum $\Pi_\parallel=\hbar\mathbf{K}_\parallel$ is an exact integral of motion,[7] which implies that the slow motion of the c.m. is decoupled from the fast relative motion in Eq. (2). Therefore, the exciton wave function can be written as

$$\Phi(\mathbf{R},\mathbf{r},z_e,z_h) \rightarrow \exp[i\mathbf{K}_\parallel\cdot\mathbf{R}]\varphi(\mathbf{r},z_e,z_h). \tag{3}$$

Because of the strong confinement along the z direction, we are allowed to separate the lateral motion in the xy plane from the z motion. Further, we assume that the confinement interaction is larger than the Coulomb (i.e., exciton) interaction, which allows us to use the adiabatic approximation

$$\varphi(\mathbf{r},z_e,z_h) = \varphi_e(z_e)\varphi_h(z_h)\exp[-\alpha r^2], \tag{4}$$

where $\varphi_e(z_e)$ [$\varphi_h(z_h)$] is the electron (hole) wave function, which is the solution of Eq. (3) when neglecting the Coulomb interaction. The wave function for the relative motion of the exciton is approximated by a Gaussian, where α is a variational parameter. In the final step, we average the kinetic part and the Coulomb interaction part in the exciton Hamiltonian [see Eq. (3)] using the above wave function, minimize the total exciton energy with respect to α, and obtain the exciton energy.

(3) For the perpendicular magnetic field direction ($\mathbf{B}_\perp\|\hat{z}$), the local well width fluctuations will influence the diamagnetic shift much more, the reason being that the exciton will be trapped in such local well width fluctuations. For such a weakly confined exciton, there will be a competition between the magnetic confinement and the localization due to well width fluctuations. A local increase of the well width results in a lower zero point energy for the electron and the hole, which can be viewed as an attractive potential well in the plane of the QW.[11–14] For example, for $h=3$ ML and a local well with an increase of 1 ML, the difference in zero point energy for the electron (hole) is $\Delta V_e=40$ (50) meV. The corresponding results for $h=4$ ML is $\Delta V_e=39$ (36) meV. Normally, one would expect a larger difference in zero point energy for the electron than for the hole, which is the case for $h=4$ ML. However, for the very narrow QW, the electron ground state energy is close to the conduction band offset causing $\Delta V_e<\Delta V_h$, as we found for $h=3$ ML. We use a mean field theory in the Hartree approximation to describe our system. Due to the axial symmetry of the problem, the

wave function of the particles can be written as $\Psi(\rho, z, \theta) = \psi(\rho, z)e^{-il\theta}$. The electron and the heavy-hole states in the QW are obtained by solving the following 2D Schrödinger equations:

$$\left[-\nabla_{ze}\frac{\hbar^2}{2m_e(z_e)}\nabla_{ze} - \frac{\hbar^2}{2m_e}\left(\nabla_{\rho e}^2 + \frac{1}{\rho_e}\nabla_{\rho e}\right) + \frac{\hbar^2}{2m_e}\frac{l_e^2}{\rho_e} - \frac{l_e}{2}\frac{\hbar eB_\perp}{m_e c} \right.$$
$$\left. + \frac{e^2 B_\perp^2 \rho_e^2}{8m_e c^2} + V_e(\rho_e, z_e) + U_{eff}(\rho_e, z_e) \right]\psi_e(\rho_e, z_e)$$
$$= E_e \psi_e(\rho_e, z_e), \qquad (5)$$

$$\left[-\nabla_{zh}\frac{\hbar^2}{2m_h(z_h)}\nabla_{zh} - \frac{\hbar^2}{2m_h}\left(\nabla_{\rho h}^2 + \frac{1}{\rho_h}\nabla_{\rho h}\right) + \frac{\hbar^2}{2m_h}\frac{l_h^2}{\rho_h} + \frac{l_h}{2}\frac{\hbar eB_\perp}{m_h c} \right.$$
$$\left. + \frac{e^2 B_\perp^2 \rho_h^2}{8m_h c^2} + V_h(\rho_h, z_h) + U_{eff}(\rho_h, z_h) \right]\psi_h(\rho_h, z_h)$$
$$= E_h \psi_h(\rho_h, z_h), \qquad (6)$$

where $\rho_{e(h)} = \sqrt{x_{e(h)}^2 + y_{e(h)}^2}$, $V_{e(h)}(\rho_{e(h)}, z_{e(h)})$ is the confinement potential of the electron (hole), which takes into account the QW width fluctuation, and $U_{eff}(\rho_{e(h)}, z_{e(h)})$ is the effective Hartree potential felt by the electron (hole),

$$U_{eff}(\rho_{e(h)}, z_{e(h)}) = -\frac{e^2}{\varepsilon}\int \rho_{h(e)}d\rho_{h(e)}\int dz_{h(e)}$$
$$\times \int d\theta_{h(e)}\frac{|\psi_{h(e)}(\rho_{h(e)}, z_{h(e)})|^2}{\sqrt{\rho_e^2 + \rho_h^2 - 2\rho_e\rho_h\cos(\theta_e - \theta_h) + (z_e - z_h)^2}}. \qquad (7)$$

To solve self-consistently the single-particle differential equations (Eqs. (5) and (6)), we have to evaluate a threefold Hartree integral, which is given by Eq. (7). The integration over the angle θ was performed analytically, and the part which contains the ρ and z dependence was performed numerically using the logarithmically weighted method.[24] In the final step, we calculate the exciton energy as follows:

$$E_{ex} = E_e + E_h + \frac{e^2}{\varepsilon}\int \frac{|\psi_e(\rho_e, z_e)|^2 |\psi_h(\rho_h, z_h)|^2}{\sqrt{(\rho_e - \rho_h)^2 + (z_e - z_h)^2}}, \qquad (8)$$

where the last term also equals $(E_e' + E_h' - E_e - E_h)/2$, with the single-particle energies E_e' and E_h' obtained from Eqs. (5) and (6) by neglecting the Hartree potential. Note that this term defines the Coulomb interaction energy, but its value has the opposite sign (the Coulomb interaction energy is negative).

The input parameters used in our simulations for the InAs/InP material are taken from Ref. 4, except for the nonparabolicity parameter α.

III. EXPERIMENTAL SETUP

The samples were grown by solid-source molecular beam epitaxy (MBE). For the QW sample, 4 ML of InAs were deposited (1 ML is 3 Å), followed without interruption by a 20 nm thick InP barrier, both at 485 °C. The fast growth rate of 1 ML/s and the absence of interruption between InAs and
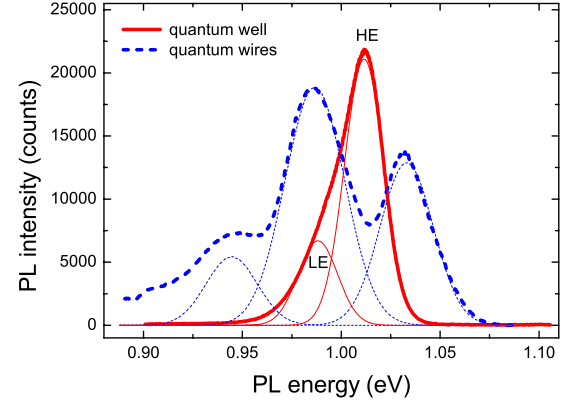

FIG. 2. (Color online) Photoluminescence spectra of the InAs/InP quantum well and wires at 20 K. The thick full (red) and dashed (blue) curves correspond to the PL energies of the well and wires, respectively. The thin full and dashed lines are Gaussian fits to the spectrum.

InP growth inhibit the kinetics, and thus no wires were formed. This is confirmed by the reflection high-energy electron diffraction (RHEED) signal, which showed a 2×4 pattern during InAs growth, corresponding to a 2D layer. For the QWRs sample, 1.7 ML of InAs was deposited at 0.1 ML/s and 515 °C in a pulsed dynamic way (pulsed In sequence: 1 s on and 2 s off). The deposition of InAs was interrupted immediately after the change from 2D to three-dimensional growth was observed in the RHEED pattern. Then, the sample was kept 1 min under As pressure and finally covered by a 20 nm thick InP layer grown at 1 ML/s. PL measurements were performed in a He bath cryostat at 4.2 K and in a He flow cryostat (20–200 K). Excitation of the samples was achieved by a solid-state laser operating at 532 nm via a 200 m core optical fiber. The laser power was controlled between 0.6 and 600 mW by neutral density filters corresponding to power densities at the sample from 0.06 to 60 W cm^{-2}. The luminescence, collected by six surrounding fibers, was analyzed in a 0.25 m spectrometer with a liquid-nitrogen cooled InGaAs detector. A magnetic field of 50 T is obtained by pulsed fields. During a 25 ms magnetic field pulse, up to 23 spectra were taken at various fields with a photon integration time of 0.2 ms each.

IV. COMPARISON OF VERTICAL CONFINEMENT IN QUANTUM WIRES AND WELLS

The QWR structure shows three distinct PL peaks [see the thick dashed (blue) curve in Fig. 2]. From our previous theoretical study of such quantum wires,[4] we know that they correspond to a wire height of 4–6 ML and a width of 180 Å. The temperature dependence of these three PL lines is similar to that reported by Fuster et al.[25] on a similar sample, revealing a unipolar electron escape toward the barrier at room temperature. We also note that in our sample, the intensity of the low-energy peak originating from the 6 ML thick wires increases up to 80 K, evidencing the occurrence of phonon assisted tunneling or recapture of carriers that
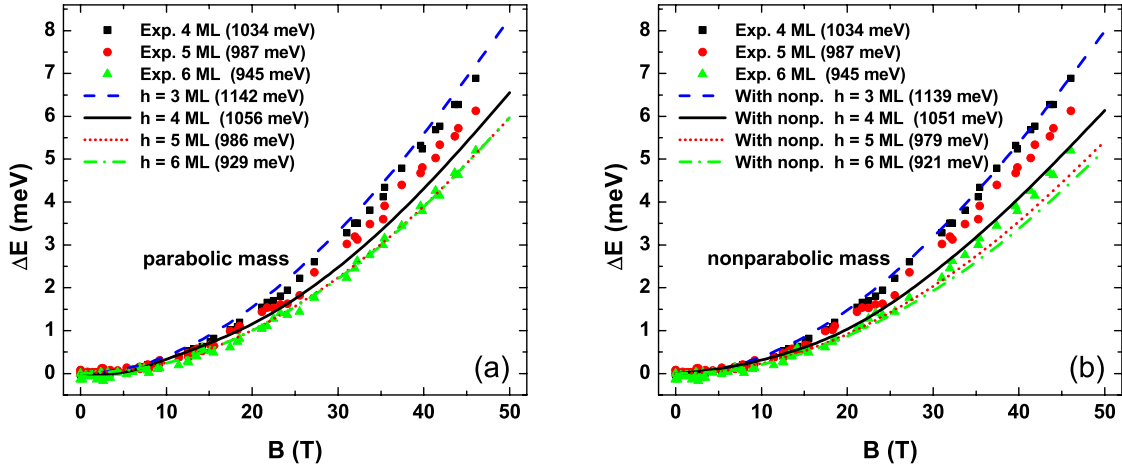
FIG. 3. (Color online) The exciton diamagnetic shift as a function of magnetic field ($\mathbf{B} \parallel [110]$) for InAs/InP quantum wires. The dashed (blue), full (black), dotted (red), and short dash-dot (green) curves correspond to our numerical results with parabolic mass of the electron (a) and when the effect of band nonparabolicity is included (b) for different heights of the wire. The full squares (black), circles (red), and triangles (green) represent the experimental data for the wire height 4, 5, and 6 ML, respectively, and width equal to 180 Å. The value of the experimental and the calculated PL energies in the absence of the magnetic field are given in parentheses.

have thermally escaped from thinner wires.[25]

In Fig. 3, we compare the theoretical results of the exciton diamagnetic shift $[\Delta E = E(B) - E(0)]$ in the InAs/InP QWR, which are denoted by four curves corresponding to the wire height $h = 3–6$ ML and width $w = 180$ Å, with the experimental data, which are denoted by three different symbols. The numerical calculations for the electron parabolic effective mass and the electron nonparabolic effective mass are shown [see Figs. 3(a) and 3(b)]. Note that the experimental data in Fig. 3 differ slightly from those reported in our previous works[4,16] due to different growth conditions of the QWR. However, the theoretical results for the electron parabolic effective mass, when height h equals 3–5 ML, are the same as those given in Ref. 4. The theoretical results for the bulk (parabolic) mass of the electron in Fig. 3(a) only slightly differ from those in Fig. 3(b). However, in the case of parabolic electron effective mass, we obtained a better agreement between the theoretical result and experimental data of the same height h, as compared to the case of nonparabolic electron effective mass. The best agreement in the whole B region is found when $h = 6$ ML [compare the dashed-dot (green) curve with the full triangles (green) in Fig. 3(a)]. For the height of 4 and 5 ML, we see a fair agreement in Fig. 3(a) between the experimental points and the theoretical curves. At 45 T, a discrepancy of 1.3 meV for $h = 4$ ML and 1.0 meV for $h = 5$ ML is observed. The reason for these small deviations is probably due to the fact that we assume a rectangular shape of the QWR in our theoretical model, which may not be the exact experimental shape.[16] Comparing the theoretical and experimental PL energies for different heights of the wire at zero magnetic field in Fig. 3(b), we see a difference of about 24 meV for the wire height $h = 6$ ML and a smaller difference for $h = 4–5$ ML. When we compare the computed PL energies with the experimental PL energies for the parabolic mass of the electron in Fig. 3(a), we found that the 5 ML computed PL energy $E_{PL(5 \text{ ML})} = 986$ meV is closer to the experimental one $E_{PL(expt \ 5 \text{ ML})} = 987$ meV, as com-

pared to the calculated and experimental PL energies for the height of 4 ML, $E_{PL(4 \text{ ML})} = 1056$ meV and $E_{PL(expt \ 4 \text{ ML})} = 1034$ meV, and the height of 6 ML, $E_{PL(6 \text{ ML})} = 929$ meV and $E_{PL(expt \ 6 \text{ ML})} = 945$ meV.

When the magnetic field is applied along the [110] direction, the confinement properties in the direction of the wire height are investigated. The diamagnetic shift in the range of B between 0 and 50 T increases with decreasing wire height for both theoretical and experimental results shown in Fig. 3. This indicates a larger exciton wave function extent for smaller wires. To illustrate this, we calculated the wave function radii in the InAs/InP QWR theoretically. In Table I, we present a list of the wavefunction radii for the electron and heavy hole along the [001] direction of the QWR with $h = 4–6$ ML, where we define the particle radius as the average quadratic distance along the [001] direction of the wire $\rho_{gr} = \sqrt{\langle y^2 \rangle}/2$. Note that the electron extent ρ_{gr_e} decreases with increasing well width, while the opposite behavior is found for the hole extent $\rho_{gr_{hh}}$. The unusual behavior for the electron extent is a consequence of the electron wave function

TABLE I. Wave function radii for the electron (ρ_{gr_e}), the heavy hole ($\rho_{gr_{hh}}$), and the exciton ($\rho_{gr_{exc}}$) along the *growth* direction of the InAs/InP quantum well (z direction) with width of 3–5 ML and the InAs/InP quantum wire ([001] direction) with height of 4–6 ML.

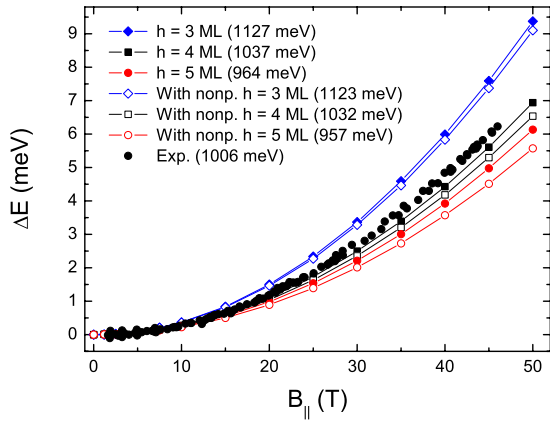|	ρ_{gr_e} (Å)	$\rho_{gr_{hh}}$ (Å)	$\rho_{gr_{exc}}$ (Å)
QW 3 ML	9.0	2.4	9.3
QW 4 ML	7.5	2.5	7.9
QW 5 ML	6.9	2.7	7.4
QWR 4 ML	7.7	2.6	8.1
QWR 5 ML	7.0	2.7	7.5
QWR 6 ML	6.7	3.0	7.3

FIG. 4. (Color online) The exciton diamagnetic shift as a function of parallel magnetic field ($\mathbf{B}_\parallel \perp \hat{z}$) for InAs/InP quantum wells. The curves with the open and closed symbols correspond to the exciton diamagnetic shift with and without taking into account the effect of band nonparabolicity for the electron, respectively. The curves with the diamonds (blue), squares (black), and circles (red) correspond to the quantum well with width of 3, 4, and 5 ML, respectively. The full circles (black) correspond to the experimental data. The value of the experimental and the calculated PL energies in the absence of the magnetic field are given in parentheses.

spillover effect. As a result, also the exciton size increases with decreasing well width (see the data for $\rho_{gr_{exc}}$ in Table I).

In Fig. 4, we examine the exciton diamagnetic shift for the InAs/InP quantum well when the magnetic field is applied perpendicular to the z direction. The PL experiments show that the QW structure clearly has a main peak, high-energy (HE) peak, and a second PL peak, low-energy (LE) peak, about 20 meV below [see the full (red) curves Fig. 2]. We compare the theoretical results for the QW with widths equal to 3, 4, and 5 ML, with the experimental data of the HE peak denoted by the full circles (the diamagnetic shift of the LE peak was not measured). Band nonparabolicity has a small effect on the results (compare the curves with open and closed symbols in Fig. 4). The effect of band nonparabolicity

is to increase the electron effective mass. The exciton diamagnetic shift is inversely proportional to the reduced mass of the electron and heavy hole; therefore, the exciton diamagnetic shift when including the nonparabolic electron mass is smaller than the one with the bulk electron mass. Up to $B_\parallel = 30$ T, the calculated diamagnetic shift energies (when the effect of the nonparabolicity is included) for the QW with width of 4 ML are in close agreement with the experimental data. At 45 T, the discrepancy between theory and experiment is only 0.7 meV. When comparing the calculated PL energies at zero magnetic field (when including band nonparabolicity), we found that the 4 ML results $E_{PL(4\ ML)} = 1032$ is closest to the experimental PL energy $E_{PL(expt)} = 1006$ meV (we assumed a bulk band gap energy for InAs of $E_g = 472$ meV). This is consistent with the fact that the 4 ML results also give the best agreement for the exciton diamagnetic shift and with the intended thickness of the QW in the MBE growth. From Fig. 4, we see that the calculated diamagnetic shift increases with decreasing well width. The diamagnetic shift is determined by the lateral size of the wave function perpendicular to the magnetic field. In the case of the parallel magnetic field, it reflects the exciton extent along the z direction of the QW. We found a large wave function spillover in the growth direction of the well.

Figure 5 shows the density of the electron (when the effect of band nonparabolicity is included) and heavy hole along the z direction. Because the QW is very thin and the electron mass is at least six times smaller along the z direction than the heavy-hole mass, the largest part of the electron density is in the barrier of the QW in contrast to the heavy-hole density, which is mostly situated in the well. The wave function radii for the particles along the growth direction of the QW ($\rho_{gr} = \sqrt{\langle z^2 \rangle}/2$) with $h = 3-5$ ML are listed in Table I. When compared to the theoretical results of the exciton extent in the QWR with the one in the QW (see Table I), we found that the extent of the electron, heavy hole, and exciton along the z direction for the QW with $h = 4$ and 5 ML is slightly smaller than the corresponding extent along the [001] direction for the QWR with $h = 4$ and 5 ML. The electron and the exciton wave function spillover was found in
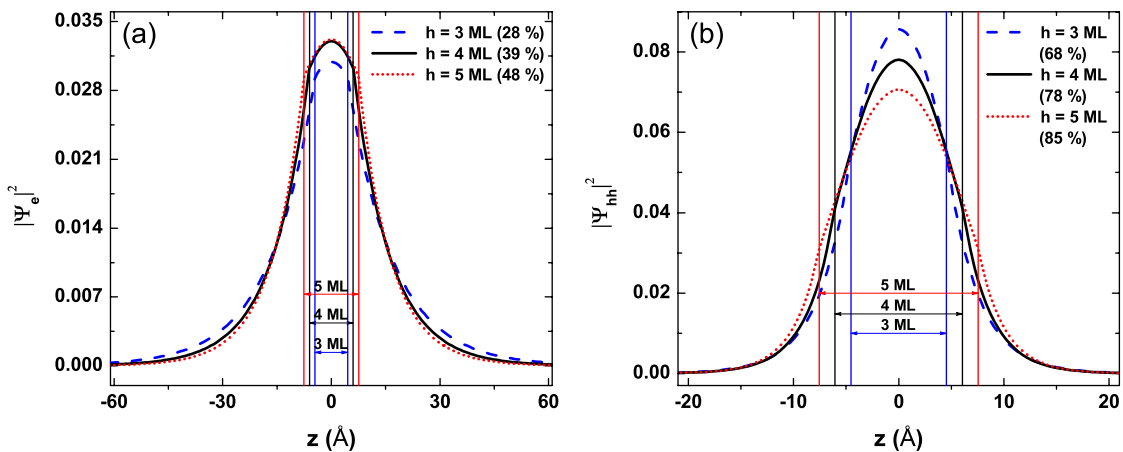

FIG. 5. (Color online) The probability density for the electron (a) and the heavy hole (b) along the growth direction (z direction) in a InAs/InP quantum well with widths 3, 4, and 5 ML (the dashed (blue), full (black), and dotted (red) curves, respectively). The probability of the electron and the heavy hole to be inside the quantum well is indicated in parentheses.

TABLE II. The exciton reduced mass (m_0 is the vacuum electron mass) along the z direction of the InAs/InP quantum well and quantum wire with and without including the effect of band nonparabolicity.

	μ_{par} (m_0)	μ_{nonp} (m_0)
QW 3 ML	0.042	0.051
QW 4 ML	0.036	0.047
QW 5 ML	0.033	0.044
QWR 4 ML	0.037	0.047
QWR 5 ML	0.033	0.044
QWR 6 ML	0.031	0.042

both QW and QWR, but not for the heavy hole (see Table I), which proves that the exciton extent is predominantly determined by the electron extent. We also found that along the z direction of the QW with different h, the effective mass of the exciton is different. From Table II, we can see a larger exciton effective mass μ for the thinner well[26] (we also give a list of exciton effective masses for the QWR), where for the QW,

$$\frac{1}{\mu} = \int dz_e dz_h |\varphi_e(z_e)|^2 |\varphi_h(z_h)|^2 \left(\frac{1}{m_e(z_e)} + \frac{1}{m_h(z_h)} \right), \quad (9)$$

and for the QWR,

$$\frac{1}{\mu} = \int dx_e dy_e dx_h dy_h |\Psi_e(x_e, y_e)|^2 |\Psi_h(x_h, y_h)|^2$$
$$\times \left(\frac{1}{m_e(x_e, y_e)} + \frac{1}{m_h(x_h, y_h)} \right). \quad (10)$$

The QW shows a second PL peak about 20 meV below the main peak (Fig. 2). This LE peak can be attributed to a monolayer fluctuation in the QW thickness. The observation of the LE shoulder is very surprising since QW excitons can typically migrate to regions with the largest well thickness (and so to regions of the lowest confinement energy) at helium temperature. We assume that the exciton energy state corresponding to the main PL peak (HE peak) is a local minimum originating from the predominant thickness of $h = 4$ ML, while the LE state is attributed to 5 ML thickness fluctuations that are less abundant [Figs. 7(a) and 7(b)]. The ratio of the intensities of the 4 and 5 ML peaks does not depend on the laser power at 20 K (see Fig. 6). Hence, we conclude that the charge carriers in the QW are trapped by thickness fluctuations and that there is no coupling between the optically active 4 and 5 ML fluctuations. Therefore, these states are spatially well separated. Indeed, charge carriers that are in a region of 4 ML well thickness, which is close to 5 ML fluctuation, would not significantly be optically active since such charge carriers would easily migrate toward the 5 ML fluctuation. Since there is no coupling at 20 K, the ratio of the peak intensities reflects the ratio of the number of corresponding states: There are 3.3 times more optically active 4 ML states than 5 ML states. When temperature T increases, the 4 ML peak (HE peak) loses intensity in favor of
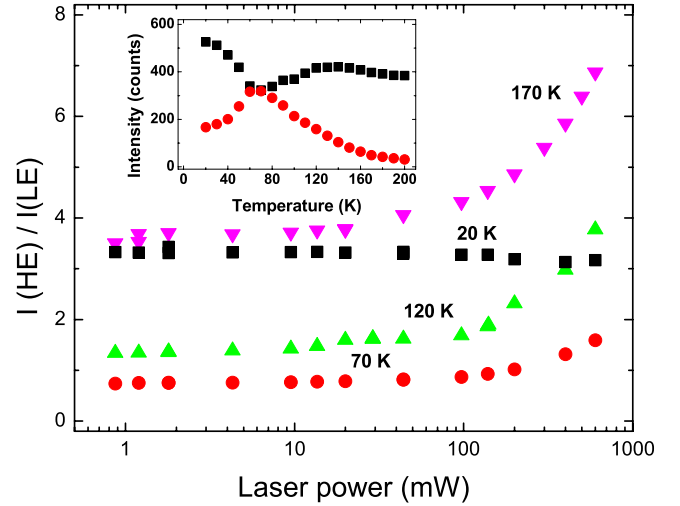

FIG. 6. (Color online) Laser power dependence of the ratio of the intensities of the HE and LE peaks of the quantum well at the different temperatures denoted by the different symbols. At 20 K, this ratio remains constant with varying laser power. With increasing temperature, the laser power dependence becomes more pronounced. The inset shows the temperature dependence of the absolute intensities of the HE [squares (black)] and LE [circles (red)] peaks.

the 5 ML peak (LE peak), as shown in the inset of Fig. 6. So, in the QW, we find a phonon assisted tunneling or the recapture of carriers that have thermally escaped from the thinner regions of the QW [see Fig. 7(c)]. For temperatures above about 70 K, the 4 ML peak regains some of its relative intensity as the laser power increases (see Fig. 6), indicating that the thermal redistribution rate is smaller than the rate at which the charge carriers are injected at elevated laser power.
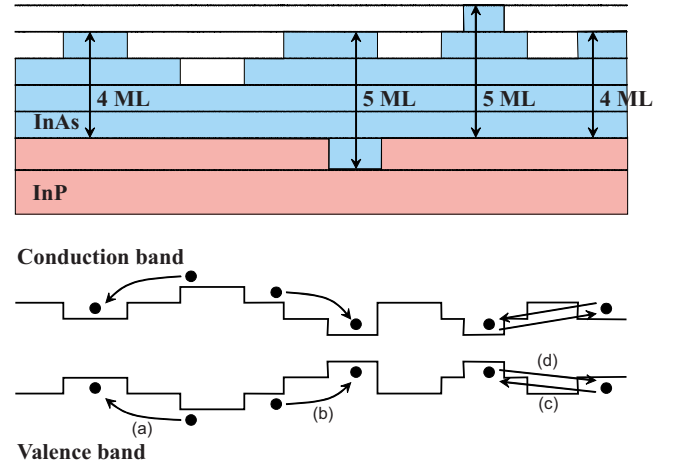

FIG. 7. (Color online) Schematic diagram of the thickness fluctuations within the quantum well (top) and the band structure (bottom). Most excitons can freely move to the most abundant 4 ML fluctuation at all temperatures (a), and some excitons get trapped by a 5 ML fluctuation (b). At moderate temperature excitons are able to migrate from the 4 ML to the 5 ML state (c). At temperatures above 70 K, thermal redistribution causes excitons to migrate from the 5 ML to the 4 ML state (d).
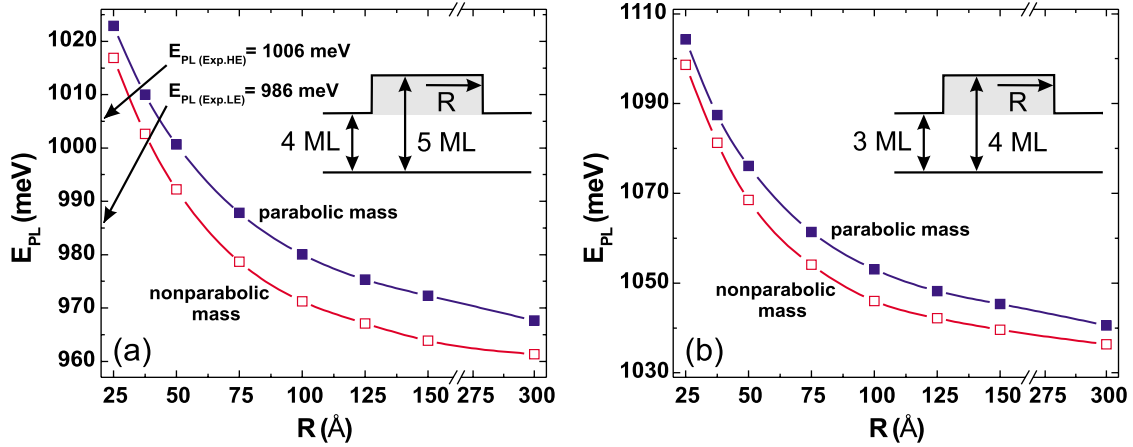
FIG. 8. (Color online) The PL energy as a function of the fluctuation radius R for InAs/InP quantum well with width of 4 ML (a) and 3 ML (b), and fluctuation of 1 ML with the profile shown in the inset of each graph. Symbols are the calculated points and the curves are guides to the eye. The experimental PL energy of the HE and LE peaks is indicated in the inset of graph (a).

The 5 ML peak has a maximum relative intensity at 70 K, after which the thermal activation to the 4 ML fluctuations starts to dominate [Fig. 7(d)]. At 170 K, the intensity ratio is the same as at 20 K at low laser power, indicating that charges can now move around freely and that their distribution reflects the density of states (i.e., the intensity ratio equals the ratio of available states). 170 K corresponds quite well with the 20 meV peak separation ($k_B T = 14.6$ meV for temperature $T = 170$ K). We also found that the intensity of the 4 ML peak at 200 K retains 70% of the intensity at 20 K. Because of unclarity regarding the dimensions of the well with due to thickness fluctuations, it motivated us to study the excitonic properties in the QW with local well width fluctuations.

V. WIDTH FLUCTUATIONS IN QUANTUM WELL

Here, we study the influence of the InAs/InP quantum well width fluctuation on the electron–heavy-hole transition (PL) energy. As was mentioned previously, the closest theoretical PL energy to the experimental PL energy of the HE peak is for a QW with width 4 ML. Therefore, theoretically, we investigate the QW with width of 4 ML and a fluctuation of 1 ML (let us call it a 4-5 QW) and with width of 3 ML and fluctuation of 1 ML (let us call it a 3-4 QW), as shown in the inset in Figs. 8(a) and 8(b), respectively. We compute the PL energy for 3-4 and 4-5 QWs as a function of the fluctuation radius R and compare it with the experimental PL energies of the HE and LE peaks. Besides, we present the results using the bulk (parabolic) mass of the electron and the results when including the effect of band nonparabolicity. The best fit for the 4-5 QW is found when the fluctuation radius is between 25 and 50 Å, as we can see in Fig. 8(a). For larger fluctuation radii R, the PL energy of the ground state decreases, as expected. The calculated PL energies for the 3-4 QW are above the experimental PL energies of the HE and LE peaks even when the fluctuation radius is $R = 300$ Å, whose PL energy $E_{PL(300\ \text{Å})} = 1036$ meV is close to that of the 4 ML well $E_{PL(4\ \text{ML})} = 1032$ meV.

In the next step, we calculated the electron–heavy-hole Coulomb interaction energy dependence on the quantum well width fluctuation radius for the 4-5 QW. In Fig. 9, the Coulomb energy between electron and heavy hole in the ground state is shown. We present the results for a parabolic effective mass (the curve with full squares in Fig. 9) and nonparabolic electron effective mass (see the curve with open squares). The size of the Coulomb interaction energy is larger when band nonparabolicity is included because of the smaller electron effective mass. The largest absolute value of both energies decrease continuously up to $R = 75$ Å in case of parabolic mass, and up to $R = 50$ Å when the effect of band nonparabolicity is included. The reason for such an energy decrease at small R is the spillover of the electron wave function. This is also demonstrated in the inset of Fig. 9, where we show that the electron density for the $R = 50$ Å is more squeezed than that for $R = 25$ Å. The electron density
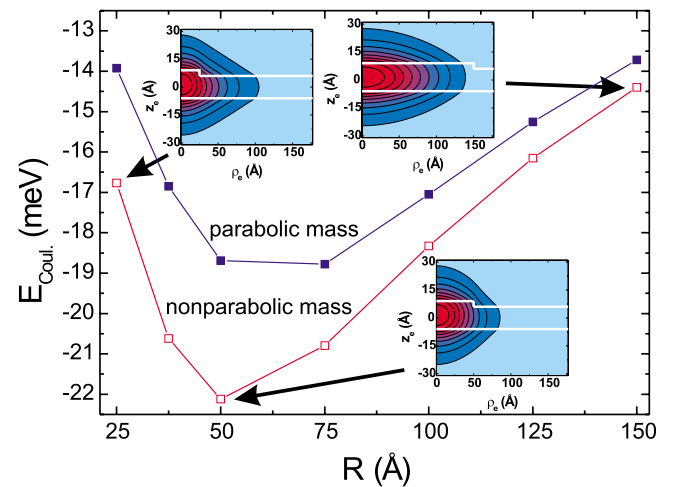

FIG. 9. (Color online) The electron–heavy-hole Coulomb interaction energy as a function of the fluctuation radius R for InAs/InP quantum well with width of 4 ML and fluctuation of 1 ML. The insets show contour plots of the electron density for $R = 25$, 50, and 150 Å.
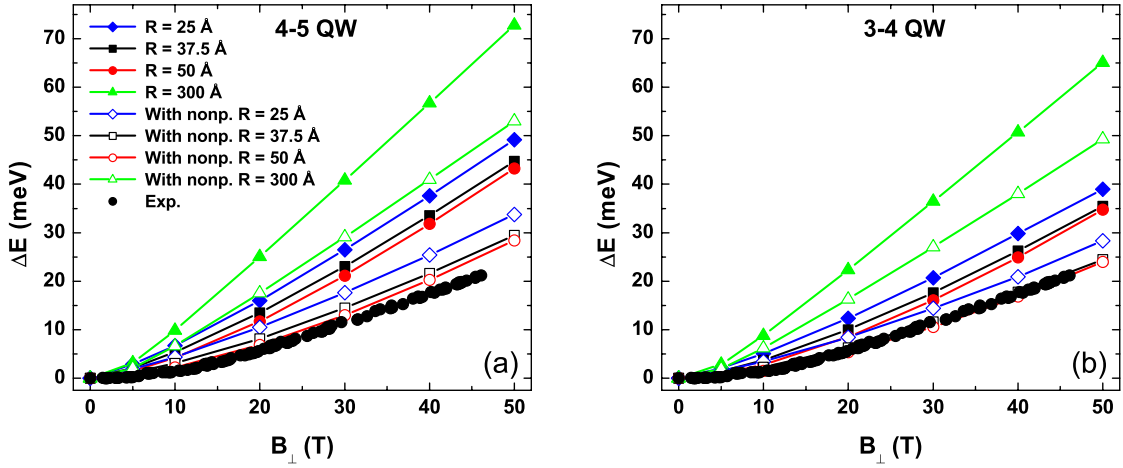
FIG. 10. (Color online) The exciton diamagnetic shift as a function of perpendicular magnetic field ($\mathbf{B}_\perp \| \hat{z}$) for InAs/InP quantum well. The curves with the open and closed symbols correspond to the exciton diamagnetic shift with and without taking into account the effect of band nonparabolicity for the electron. The curves with the diamonds (blue), squares (black), circles (red), and triangles (green) correspond to the quantum well with width of 4 ML, fluctuation width of 5 ML (a), and the fluctuation radius of 25, 37.5, 50, and 300 Å, respectively. In graph (b), the same identification of the curves is used as in graph (a), but now for the quantum well with width of 3 ML and fluctuation width of 4 ML. The full circles (black) correspond to the experimental data.

for $R = 150$ Å is the most prolongated in comparison to the previous two radii, as expected, because the radius of the fluctuation increases; i.e., the electron is less localized in the plane.

Let us examine the exciton diamagnetic shift in the InAs/InP QW with the local width fluctuations in the presence of a magnetic field parallel to the growth direction ($\mathbf{B}_\perp \| \hat{z}$). In Figs. 10(a) and 10(b), we compare the theoretical results of the exciton diamagnetic shift for the 4-5 and 3-4 QWs with the experimental results of the HE peak [see the curves with the symbols and the full circles (black) in Fig. 10, respectively]. We present the calculations with and without inclusion of band nonparabolicity (see the curves with the open and closed symbols in Fig. 10, respectively) when the QWs fluctuation radii are in the range of 25 and 300 Å for both the 3-4 and 4-5 QWs. Again, we observe a smaller diamagnetic shift for the case when nonparabolicity for the electron is included than in the case when it is excluded, as seen previously for the parallel magnetic field (see Fig. 4), but now the effect is much larger. Up to 30 T, we found the best agreement between theory and experiment for the 4-5 QW with a well width fluctuation radius $R = 50$ Å, while a full agreement in the whole B region is achieved for the 3-4 QW with the same well width fluctuation radius [compare the curves with the open circles (red) and experimental points in Figs. 10(a) and 10(b)]. Nevertheless, for the 4-5 QW, the computed PL energy is within 15 meV from the experimental PL energy of the HE peak [compare the curve with the open symbols (red) for $R = 50$ Å and the experimental value of the PL energy in Fig. 8(a)], while for the 3-4 QW a difference of about 60 meV is found [compare the curve with the open symbols (red) for $R = 50$ Å and the experimental value of the PL energy in Fig. 8(b)]. Besides, for the radius of 300 Å, the diamagnetic shift is much larger than that for $R = 50$, 37.5, and 25 Å. This is a consequence of the wave function spillover effect for the electron. In the case of

the perpendicular magnetic field, the discrepancy between theory and experiment for the 4-5 QW is about 5 meV at 45 T when $R = 50$ Å. However, the exciton extent in the plane of the 4-5 QW with the radius of the fluctuation $R = 50$ Å is 6.7 nm (6.2 nm for the 3-4 QW), which is in reasonable agreement with the exciton radius found from experiment, 7.7 nm for the 4 and 5 ML QW.

VI. CONCLUSIONS

In summary, we studied theoretically and experimentally the vertical confinement in a InAs/InP self-assembled QWR and in a InAs/InP QW. The wave function radii of the electron, heavy hole, and exciton along the growth direction of the QW and [001] direction of the QWR were calculated. From a comparison with the qualitative measure of the vertical exciton extent obtained from the experimental data, we conclude that the exciton wave function spillover effect in the 3-5 ML QWs and the 4-6 ML QWRs is large.

The exciton diamagnetic shift for QW in the presence of parallel magnetic field and for QWR in the presence of magnetic field applied along the [110] direction is calculated, reflecting in both cases the confinement properties of the wire height and the well width. We obtained the best agreement between theory and experiment for the QWR with height of $h = 6$ ML, and also a fair agreement for QWR with $h = 4$ and 5 ML, when using the parabolic mass of the electron. Deviation from the experiment at $B = 45$ T is found to be less than 1.3 meV for 4 ML QWR and about 1 meV for 5 ML QWR. When comparing the PL energies and the diamagnetic shift in the QW, the best agreement is found for a 4 ML well when including the conduction band nonparabolicity effect.

Experimental results of the laser power dependence at different temperatures for InAs/InP QW indicate that the charge carriers (excitons) are trapped by the well width fluc-

tuations. Numerical results of the PL energy for the QW with local width fluctuations show that experimentally found HE and LE PL peaks correspond rather to the QW with width of 4 ML and fluctuation width of 1 ML, than to the 3 ML well with fluctuation width of 1 ML. The best agreement for the HE peak is found for the 4-5 QW when the fluctuation radius R is between 25 and 50 Å. The calculated exciton diamagnetic shift in the presence of a perpendicular magnetic field for both 3-4 and 4-5 QWs with $R=37.5-50$ Å, when using the nonparabolic effective mass of the electron, fits best the experimental obtained diamagnetic shift of the HE peak.

[1] F. V. Kyrychenko and J. Kossut, Phys. Rev. B **61**, 4449 (2000).

[2] G. W. Bryant and Y. B. Band, Phys. Rev. B **63**, 115304 (2001).

[3] J. R. Madureira, M. Z. Maialle, and M. H. Degani, Phys. Rev. B **66**, 075332 (2002).

[4] Y. Sidor, B. Partoens, and F. M. Peeters, Phys. Rev. B **71**, 165323 (2005).

[5] M. Fritze, I. E. Perakis, A. Getter, W. Knox, K. W. Goossen, J. E. Cunningham, and S. A. Jackson, Phys. Rev. Lett. **76**, 106 (1996).

[6] K. Chang and F. M. Peeters, Phys. Rev. B **63**, 153307 (2001).

[7] B. R. Johnson, J. O. Hirschfelder, and Kuo-Ho Yang, Rev. Mod. Phys. **55**, 109 (1983).

[8] K. J. Nash, M. S. Skolnick, P. A. Claxton, and J. S. Roberts, Phys. Rev. B **39**, 10943 (1989).

[9] F. M. Peeters and J. E. Golub, Phys. Rev. B **43**, 5159 (1991).

[10] A. B. Dzyubenko and A. L. Yablonskii, Phys. Rev. B **53**, 16355 (1996).

[11] G. Eytan, Y. Yayon, M. Rappaport, H. Shtrikman, and I. Bar-Joseph, Phys. Rev. Lett. **81**, 1666 (1998).

[12] J. G. Tischler, A. S. Bracker, D. Gammon, and D. Park, Phys. Rev. B **66**, 081310(R) (2002).

[13] A. V. Filinov, C. Riva, F. M. Peeters, Yu. E. Lozovik, and M. Bonitz, Phys. Rev. B **70**, 035323 (2004).

[14] A. S. Bracker, E. A. Stinaff, D. Gammon, M. E. Ware, J. G. Tischler, D. Park, D. Gershoni, A. V. Filinov, M. Bonitz, F. M. Peeters, and C. Riva, Phys. Rev. B **72**, 035332 (2005).

[15] L. González, J. M. García, R. García, F. Briones, J. Martínez-Pastor, and C. Ballesteros, Appl. Phys. Lett. **76**, 1104 (2000).

[16] J. Maes, M. Hayne, Y. Sidor, B. Partoens, F. M. Peeters, Y. González, L. González, D. Fuster, J. M. García, and V. V. Moshchalkov, Phys. Rev. B **70**, 155311 (2004).

[17] D. Fuster, L. González, Y. González, M. U. González, and J. Martínez-Pastor, J. Appl. Phys. **98**, 033502 (2005).

[18] P. Caroff, C. Paranthoen, C. Platz, O. Dehaese, H. Folliot, N. Bertru, C. Labbé, R. Piron, E. Homeyer, A. Le Corre, and S. Loualiche, Appl. Phys. Lett. **87**, 243107 (2005).

[19] G. L. Bir and G. E. Pikus, *Symmetry and Strain-Induced Effects in Semiconductors* (Wiley, New York, 1974).

[20] Calvin Yi-Ping Chao and S. L. Chuang, Phys. Rev. B **46**, 4110 (1992).

[21] U. Ekenberg, Phys. Rev. B **40**, 7714 (1989).

[22] A. Krotkus and Z. Dobrovolskis, *Electrical Conductivity of Narrow-Gap Semiconductors* (Vilnus, Mokslas, 1988).

[23] M. Levinshtein, S. Rumyantsev, and M. Shur, *Handbook Series on Semiconductor Parameters* (World Scientific, London, 1996), Vol. 1.

[24] K. L. Janssens, B. Partoens, and F. M. Peeters, Phys. Rev. B **64**, 155324 (2001).

[25] D. Fuster, J. Martínez-Pastor, L. González, and Y. González, Phys. Rev. B **71**, 205329 (2005).

[26] C. Wetzel, R. Winkler, M. Drechsler, B. K. Meyer, U. Rössler, J. Scriba, J. P. Kotthaus, V. Härle, and F. Scholz, Phys. Rev. B **53**, 1038 (1996).